Validation of a time-dependent deterministic model for neutron noise on the first CROCUS experimental measurements

A. Brighenti[1], S. Santandrea[1], I. Zmijarevic[1*]and Z. Stankovski[1]

[1]DES/ISAS/DM2S/SERMA/LTSD
Université Paris-Saclay, CEA, Service d'études des réacteurs et de mathématiques appliquées,
91191, Gif-sur-Yvette, France

alberto.brighenti@cea.fr; simone.santandrea@cea.fr; igor.zmijarevic@cea.fr; zarko.stankovski@cea.fr

ABSTRACT

In the framework of the European project CORTEX, included in the H2020 program, the experimental campaign carried out with the CROCUS reactor, at the École Polytechnique Fédérale de Lausanne (EPFL) in Switzerland, aims at setting up methodologies and tools for the analysis and the interpretation of neutron noise in view of their industrial applications. An important part of the CORTEX project deals with code development and validation. In this paper, a new methodology for the simulation of neutron noise has been formulated and implemented in the APOLLO3 code. The method is based on an improved point-kinetics model employed in a fully heterogeneous 2D transport calculation. In this work, the theoretical derivation and the successive validation of the model are presented, comparing the Cross-Power Spectral Densities (CPSD) of measured and computed detector responses. Future work will consist in extending the application of the method to the analysis of 3D configurations, in particular for full reactor studies.

KEYWORDS: TRANSPORT CODE, NEUTRON NOISE, CROCUS, POINT KINETICS, VALIDATION

1. INTRODUCTION

Research and industry have been aware of the existence of neutron noise since the beginning of the nuclear era. However, in recent years, a new interest in neutron noise measurements and simulation has risen among the research and industrial reactor physics community, including the CORTEX H2020 European Project, in which CEA actively participates.
The objective of the project is to set up a noise-based core monitoring technique applicable to power and research reactors. In order to develop this technique, the data collected during neutron noise experimental campaign carried out in the CROCUS reactor [1] [2] are being used to validate computational tools developed by project members [3], among which the methodology and the model presented here.
In this work, the CROCUS reactor and the COLIBRI device setups are shown [4], followed by the presentation of a new approach and numerical method for the APOLLO3 code [5] for neutron noise simulations. The solver is used to compute the reaction rate oscillation amplitudes in the detector locations. The calculated signals are post-processed to retrieve the CPSDs that are compared with measurements.

2. EXPERIMENTAL SETUP

2.1. CROCUS reactor and COLIBRI

CROCUS is an experimental nuclear reactor used for research and teaching purposes, in the context of reactor physics and detection of ionizing radiation exercises. The reactor limited power of 100 W (so-called "zero power" reactor) turns out to be a big advantage, since few hours after the reactor shutdown, the operators can approach the core without risk of exposure. With a height of about 100 cm and a diameter of

about 58 cm, the reactor core has an almost cylindrical shape. The reactor core is constituted of two different fuel regions: the outer one is composed of metallic uranium fuel while the central one is constituted of ceramic uranium fuel pins, see Figure 1 and Table 1. All pins have an aluminum cladding and they are kept in position by means of an upper and lower grid, located about 100 cm apart, approximately corresponding to the active length of the pins. Two cadmium layers of 0.5 mm are embedded in the grids and used to reduce axial leakages. The core is contained in an aluminum tank with a diameter of about 130 cm, filled with light water acting as moderator and neutron reflector. The reactivity of the reactor is controlled by means of varying the water level and using the boron control rods. Finally, the COLIBRI device is installed in the reactor to oscillate a set of maximum 6×3 fuel pins, producing variations of neutron flux that are then recorded by the detectors. For further details about the COLIBRI design and operation refer to [4].

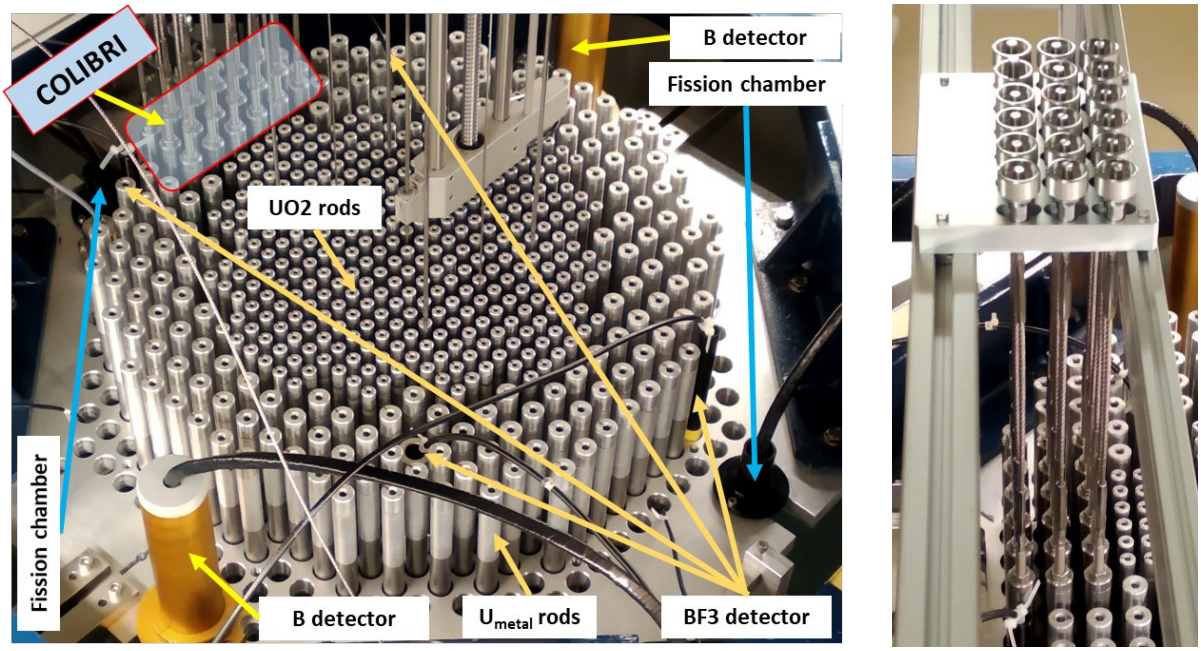

Figure 1. (a) View of the CROCUS reactor with the indication of its main components (b) zoom on the COLIBRI device.

Table 1. Main characteristics of the uranium fuel rods in the CROCUS reactor during noise experiments [6].

Type	Number [-]	Enrichment [%]	Pitch [cm]
UO_2	336	1.806	1.837
U_{metal}	176	0.947	2.917

2.2. Detectors and measurements

To monitor neutron noise amplitude during the experiments, eleven detectors are installed in various locations inside the reactor, see Figure 1a and Table 2. Each measurement record lasts a sufficiently long time to cover several cycles of the COLIBRI device, and therefore of the flux oscillations. Measurements from the detectors are collected using three different data acquisition systems, provided by EPFL and referred to as EPFL, TUD and ISTec, with the last chosen as reference for the comparisons with the simulations. Before going further in the analysis of the data, it is necessary to point out that, unfortunately, during several tests, there were issues with some detectors, which were either affected by large electronic noise, unreliable or unavailable during the entire campaign (e.g. Det#1, Det#2) [7].

Table 2. List of the available detectors installed in the CROCUS reactor [6].

Det#	Type[$]	Brand	Sensitive material	Sensitivity	Location X[&] [mm]	Location Y[&] [mm]
1	FC	Photonis	^{235}U coating	10^{-2} n_{th}^{-1}	+35.8	+8.7
2	FC	Photonis	^{235}U coating	10^{-2} n_{th}^{-1}	-35.8	-8.7
3	CIC	Merlin-Gerin	^{10}B coating	3×10^{-14} A.n_{th}^{-1}	-8.6	+36.35
4	CIC	Merlin-Gerin	^{10}B coating	3×10^{-14} A.n_{th}^{-1}	+8.6	-36.35
5	FC	Photonis	^{235}U coating	1 n_{th}^{-1}	-29.8	15.4
6	FC	Photonis	^{235}U coating	1 n_{th}^{-1}	+29.8	-14.7
7	PC	-	$^{10}BF_3$ gas	10^{-2} n_{th}^{-1}	-16.04	16.04
8	PC	-	$^{10}BF_3$ gas	10^{-2} n_{th}^{-1}	-27.71	-10.21
9	PC	Transcommerce Int.	$^{10}BF_3$ gas	10^{-2} n_{th}^{-1}	10.21	+27.71
10	PC	Transcommerce Int.	$^{10}BF_3$ gas	10^{-2} n_{th}^{-1}	-10.21	-27.71
11	MFC	Photonis	^{235}U coating	10^{-2} n_{th}^{-1}	0	0
[$] FC = Fission chamber, CIC = compensated ionization chamber, PC = proportional counter, MFC = miniature fission chamber						
[&] The coordinates x = 0.0 and y = 0.0 correspond to the center of the core, see [6] or Figure 2.						

3. INTERPRETATION OF EXPERIMENTAL DATA

Using different imposed amplitudes (A) and frequencies (ω_c) of oscillations [6], twenty different tests have been performed recording signals in selected detector positions. The specific tests selected for the validation exercises are reported in Figure 3. Here, the experimental data analysis accomplished by EPFL is taken as reference [8].

Table 3. Operational parameters [6] of the experiments selected for the validation exercise.

Exp. #	A [mm]	ω_c [Hz]
12	1.85	0.097
13	2.00	0.972

4. SIMULATION SETUP

4.1. APOLLO3® CROCUS reactor model

The APOLLO3® [5] code for reactor physics analysis is developed by CEA with joint financial support from Framatome and EDF. In the present work, the 2D version of the Two/Three Dimensions Transport (TDT) solver [9] based on the method of characteristics is used. The solver computes the static flux in various configurations depending on the shift amplitude of the cluster of 3 × 6 fuel pins connected to the COLIBRI device according to the values reported in [6]. To take into account the finite dimensions of the reactor and increase the representativeness of the calculations, axial leakage is estimated and accounted for in the neutron balance.

4.2. Static simulations and leakage model

Considering the heterogeneous reactor model with different pin displacements, see Figure 2, the TDT solver is used to compute the angular flux distributions by solving the critical problem defined as:

$$\tilde{\Sigma}_t \psi(\vec{r}, E, \Omega) = H\psi(\vec{r}, E, \Omega) + \frac{1}{k} F_{tot}\phi(\vec{r}, E), \quad (1)$$

where $\vec{r}$ is the spatial coordinate, E is the energy group, Ω is the direction angle, $\psi(\vec{r}, E, \Omega)$ is the angular flux, $\phi(\vec{r}, E)$ is the scalar flux, H is the scattering operator, F_{tot} is the total fission operator, k is the multiplication eigenvalue and $\tilde{\Sigma}_t$ is the equivalent total cross section of the problem. The value of the equivalent total cross section is defined as: $\tilde{\Sigma}_t(\vec{r}, E) = \Sigma_t(\vec{r}, E) + D(E)B^2$, where $\Sigma_t(\vec{r}, E)$ is the total cross section from nuclear data and the $D(E)B^2$ is the leakage coefficient times the buckling value. The DB^2 term accounting for radial and axial leakage [10] is computed by solving the critical problem on an equivalent infinite homogeneous domain (subscript h), where the homogeneous flux is the solution of the problem defined in integral form as:

$$\left(\Sigma_{t,h}(E) + D(E)B^2\right)\phi_h(E) = Q_h(E), \tag{2}$$

and where the homogenized total source Q_h is computed by summing the equivalent total fission $F_{tot,h}$and scattering H_h sources, namely:

$$Q_h(E) = \int_{V_{tot}} d\vec{r} \left(F_{tot,h}(\vec{r}, E)\phi(\vec{r}, E) + \int_{4\pi} d\Omega' \; H_h\psi(\vec{r}, E, \Omega) \right). \tag{3}$$

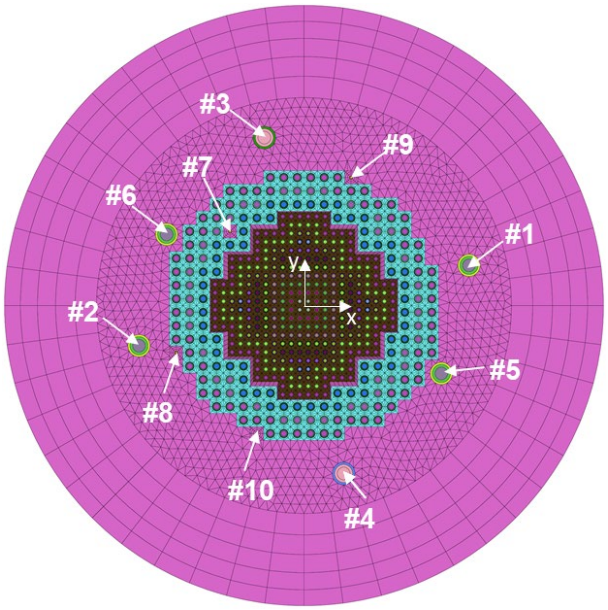

Figure 2. Computational mesh of the unperturbed CROCUS reactor and its detectors, see Table 2. The center XY of the coordinate reference system is also indicated.

The size of the initial set of static flux distributions is equal to N, corresponding to a set of points equally spaced in time during the period of oscillation, see Figure 3. By taking advantage of the symmetry of the sine curve, some of these are replicated in the remaining points. Therefore, in this specific case, to save computational time, only five points, instead of eight, are computed. The results from the static simulation are useful for anticipating what one can expect as an outcome from the noise solver in the time domain. Comparing the unperturbed geometry and the one with a maximum outward displacement, see Figure 4, the flux deviation is ~1-2% in the pins close to COLIBRI, while in the detectors of interest the variations range from ~0.04% to 0.1%. These values are expected to have the same order of magnitude as the square root of the CPSDs obtained from the noise solver. This situation is of course not an optimal preamble for the following experimental analysis, since it shows that for the installed detectors the signal will be quite low and its uncertainty may play a key role.

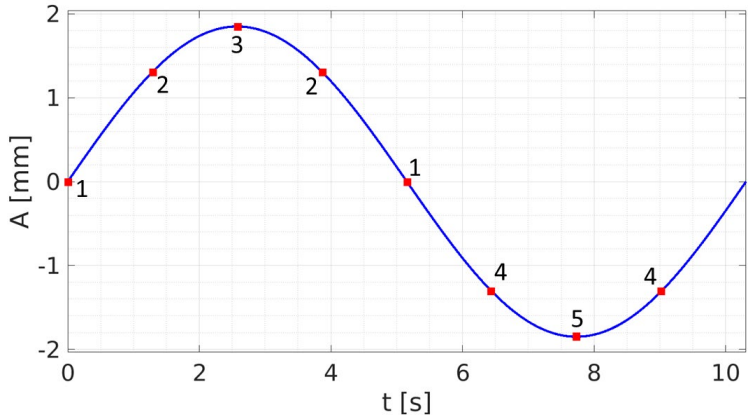

Figure 3. Ideal sine movement (blue line) with selected displacements (red squares) used in the static simulations for experiment #12 (A = 1.85 mm and ω_c = 0.097 Hz).

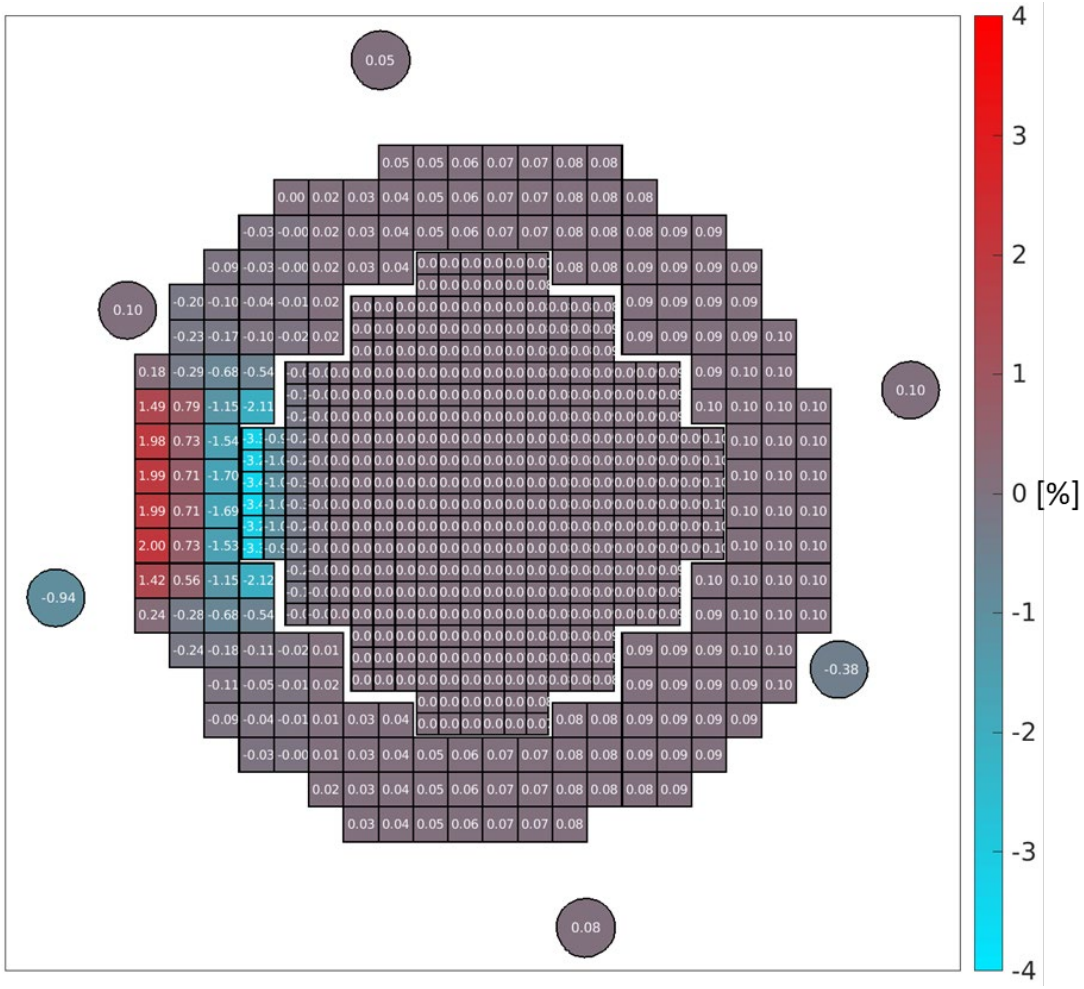

Figure 4. Pin-wise absorption rate relative difference with respect to the unperturbed configuration considering a -1.85 mm displacement for experiment #12.

4.3. The Improved Point-Kinetics model

Advancing from a previous work [11], the presented model aims at giving a more detailed representation of neutron noise in the CROCUS reactor during COLIBRI tests. The newly developed Improved Point-Kinetics model (IPK) model solves the reactor kinetics problem using a multi-group energy discretization starting from the flux and precursors concentration equations:

$$\left(\frac{1}{v}\partial_t + \Omega\cdot\nabla + \tilde{\Sigma}_t(\vec{r},E,t)\right)\psi = H\psi + \frac{F_p}{k_{dyn}}\phi + \frac{F_d\vec{C}}{k_{dyn}} \tag{4}$$

$$\partial_t C_i(\vec{r},t) = -\bar{\lambda}_i C_i(\vec{r},t) + \beta_i \int_E dE'\,\nu\Sigma_f(\vec{r},E',t)\phi(\vec{r},E',t), \tag{5}$$

where $\tilde{\Sigma}_t(\vec{r},E,t)$ is the total cross section modified accounting for the DB^2 coefficient as determined in the static calculations, $\psi = \psi(\vec{r},E,\Omega,t)$ is the angular flux, $\phi = \phi(\vec{r},E,t)$ is the scalar flux, k_{dyn} is the dynamic eigenvalue [12] representative of the stationary oscillating regime calculated over the whole period of oscillation (T), Σ_f is the macroscopic fission cross section, ν is the average number of neutrons produced by fission, β_i is the fraction of delayed neutron for family i. The term F_p refers to the prompt fission operator and $F_d\vec{C} = \sum_{i=1}^{N_d}\chi_{d,i}\lambda_i C_i$ is the contribution from the neutron precursor concentration, with C_i containing the convolution integral for the i-th precursor family with decay constant λ_i. The delayed neutron source is integrated in time using a suitable quadrature formula to account for delayed-neutron contributions, as previously discussed in [12].
In the present model, differently from [13] and from the traditional quasi-static approach (e.g. [14]), in the angular flux factorization, the shape S and power P functions preserve their energy dependence and are defined according to:

$$\psi(\vec{r},E,\Omega,t) = S(\vec{r},E,\Omega,t)\cdot P(E,t). \tag{6}$$

The normalization condition adopted for all the energy groups N_G of the IPK model is defined as:

$$\frac{1}{v_g}\langle\psi^\dagger(\vec{r},E_g,\Omega',t), S(\vec{r},E_g,\Omega',t)\rangle = 1 \quad , \quad \forall t \wedge \forall g \in [1,N_G]. \tag{7}$$

where v_g is the neutron speed in group g.
To obtain the point-kinetics equations, Eq. (4) is multiplied by a weighting function $\psi^\dagger$ and integrated over space and angle (integration is denoted by $\langle\ldots\rangle$) obtaining the general formulation of the problem:

$$\begin{aligned}\langle\psi^\dagger, \frac{1}{v}\partial_t\psi\rangle + \langle\psi^\dagger, \Omega\cdot\nabla\psi\rangle + \langle\psi^\dagger, \tilde{\Sigma}_t(\vec{r},E,t)\psi\rangle = \\ = \langle\psi^\dagger, H\psi\rangle + \frac{1}{k_{dyn}}\langle\psi^\dagger, F_p\phi\rangle + \frac{1}{k_{dyn}}\langle\psi^\dagger, F_d\vec{C}\rangle.\end{aligned} \tag{8}$$

In the present work, the weighting function is conveniently chosen as $\psi^\dagger = 1, \forall t \wedge \forall g \in [1,N_G]$ and, using the divergence theorem, the streaming term in Eq. (8) can be written for each energy group as:

$$\langle\psi^\dagger, \Omega\cdot\nabla\psi\rangle = \frac{J^+ - J^-}{\langle S/v\rangle}P. \tag{9}$$

With some manipulations, accounting for Eqs. (6) and (7), it is finally possible to obtain the balance point-kinetics equation for each energy group g:

$$\partial_t P + \frac{1}{v}\langle \partial_t S \rangle P + \frac{J^+ - J^-}{\langle S/v \rangle} P + \langle \tilde{\Sigma}_t S \rangle P - \langle HS \rangle P = \frac{1}{k_{dyn}} \langle F_p S \rangle P + \frac{1}{k_{dyn}} \langle F_d \vec{C} \rangle. \tag{10}$$

For the N initial computed static distributions, normalized according to Eq. (7), all flux points in the phase space $(\vec{x}, t)$, where $\vec{x} = (\vec{r}, E, \Omega)$, are interpolated in time over $M = L \times N$, with $L \in \mathbb{N}^+$, equally spaced points along the period, using a Fourier interpolation [15] of the kind:

$$S(\vec{x}, t) \cong c_0(\vec{x}) + \sum_{i=1}^{N/2} a_i(\vec{x}) \cos\left(\frac{2\pi}{T} t\right) + b_i(\vec{x}) \sin\left(\frac{2\pi}{T} t\right), \tag{11}$$

where the coefficients of the series (c_0, a_i and b_i) are obtained as:

$$c_0(\vec{x}) = \frac{1}{N} \sum_{j=1}^{N} S(\vec{x}, t_j) \tag{12}$$

$$a_i(\vec{x}) = \frac{2}{N} \sum_{j=1}^{N} S(\vec{x}, t_j) \cos\left(\frac{2\pi}{T} j \cdot t_j\right), \qquad j \neq N \tag{13}$$

$$a_N(\vec{x}) = \frac{1}{N} \sum_{j=1}^{N} S(\vec{x}, t_j) \cos\left(\frac{2\pi}{T} N \cdot t_j\right), \qquad j = N \tag{14}$$

$$b_i(\vec{x}) = \frac{2}{N} \sum_{j=1}^{N} S(\vec{x}, t_j) \sin\left(\frac{2\pi}{T} j \cdot t_j\right). \tag{15}$$

Concerning the temporal treatment, while the classical quasi-static method would imply the use of two different time scales for the solution of the equations for shape (coarse) and power (refined) [14], a single time scale is used to solve the transient. The final problem is a system of $M \times N_g$ equations to be solved iteratively using the power iteration method. With the converged $P(E, t)$, the angular flux is reconstructed and followed by the calculation and treatment of the detector responses.

5. VALIDATION OF COMPUTED RESULTS

5.1. Comparisons with experiments #12 and #13

In the present work, the computed results for experiments #12 and #13, see Table 3, are compared to measurements, see Figure 5 and Figure 6, respectively.

The comparisons of $CPSD_{x,5}$ (or equivalently $CPSD_{5,x}$) amplitudes, see Figure 5a and Figure 6a, show an overall good agreement between computed and experimental results of CPSDs. The model slightly underestimates the amplitude of the signals for experiment #12, possibly as a consequence of the high sensitivity of the reactor transfer function at low frequencies [16], showing that small deviations from the determined oscillation frequency ω_c may induce larger variations in the intensity of the signal. The model computes higher responses as the distance from COLIBRI decreases, showing that the spatial dependence of the results is consistent to what is expected from physics. In order to comment some experimental outcomes we can say the following: detector #3 and #10 are about the same distance from COLIBRI and one should expect to see almost the same response, as obtained by the simulation. However, this is not

necessarily true for the measurements. Again, comparing detector #3 and #4, one expects that the signal should be higher in #3 due to its proximity to the noise source, but also in this case the model and the experiment are in contradiction. Further investigations are ongoing [7]. Again, it is worth making a comment on the reported uncertainties: the estimated error bar is of the order of 10^{-6} for a relative measured reaction rate variation value of the order of 10^{-5}. By the rule of thumb, since the CPSD is the product of two signals of the same order of magnitude, it follows that the amplitude of the single detector signal is around $\sim 10^{-2}$ and its uncertainty $\sim 10^{-3}$. With these numbers in mind, one may question the capability of the detector to provide such accuracy with such a small measured value. Unfortunately, the datasheets of the installed detector are not available. Given these open issues on the measurements uncertainties, additional work is currently being carried out to address them [7]. Finally, when looking at the signal phases relative to the one of the detector pair 6&5, see Figure 6, by supposing that this pair is in phase with COLIBRI, we expect to see an increasing delay as the distance from the reference point. The only exception is represented by detector #8, the closest to the COLIBRI boundary the one which may suffer from some spectral effects [3]. For the others, the expected behavior is captured by the simulations, while the experiments show some unexpected deviations, currently under investigation. Nevertheless, we can say that the IPK model provides results in an acceptable agreement with respect to the measurements, confirming thus the good capability of the code.

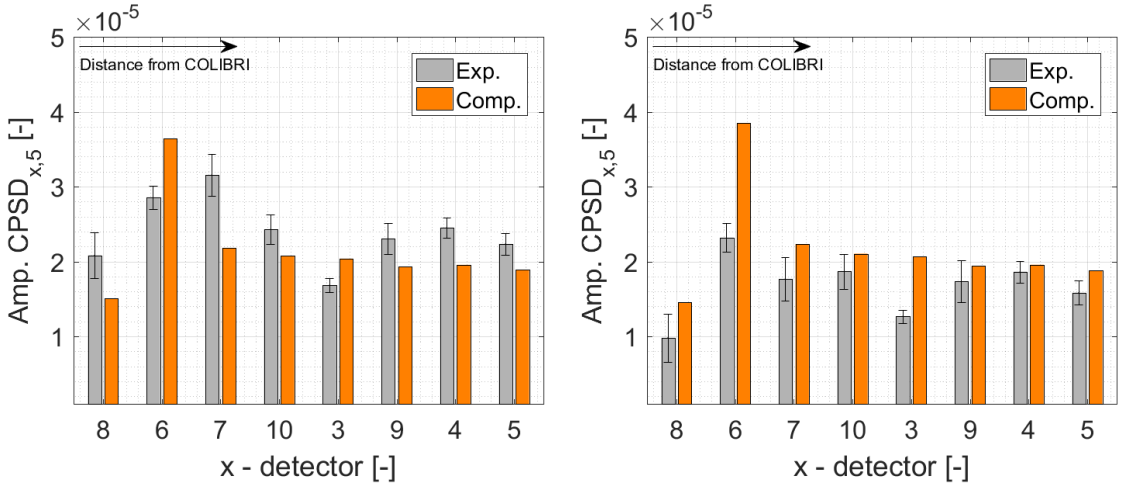

Figure 5. $CPSD_{x,5}$ amplitudes for experiments (a) #12 and (b) #13, respectively.

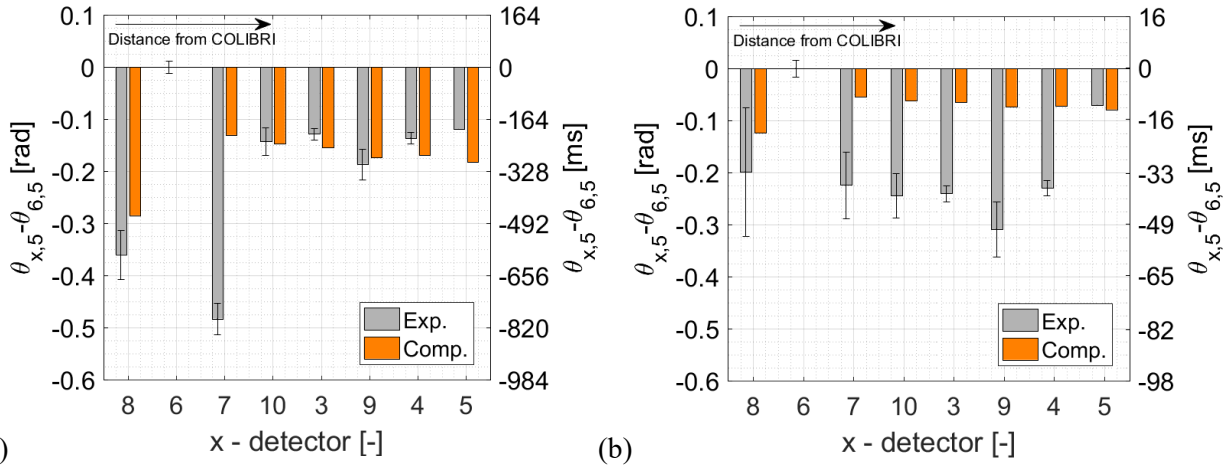

Figure 6. $CPSD_{x,5}$ relative phases for experiments (a) #12 and (b) #13, respectively.

For sake of completeness and to be consistent with analyses conducted by others [3] [8], the CPSDs of a given experiment have been normalized by the value of $CPSD_{6,5}$, see Figure 7, showing again that the code well agrees with experimental outcomes and always within the error bars when looking at experiment #13.

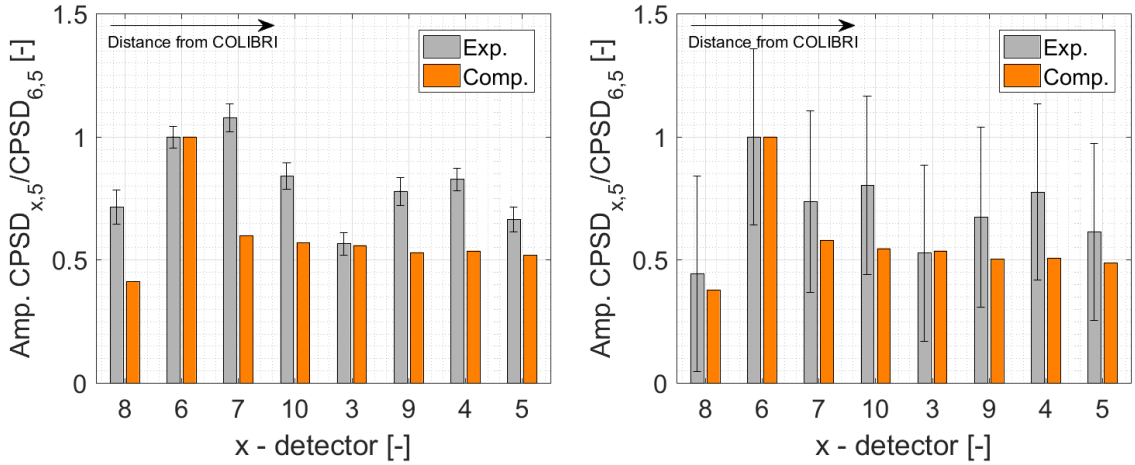

Figure 7. Normalized $CPSD_{x,5}$ amplitudes for experiments (a) #12 and (b) #13, respectively.

6. CONCLUSIONS

This paper presents the recently implemented new options for the neutron noise solver of the APOLLO3 general-purpose transport code and the application to the interpretation of the noise measurements in the COLIBRI experimental setup of the CROCUS reactor, conducted in the framework of the European CORTEX H2020 project. The approach adopted for the point-kinetics flux factorization procedure retains the energy dependency in both the shape and power. The time dependency of the space-energy distribution within an oscillation period is assessed using the fully heterogeneous transport solution in the relevant discrete instants of time. The interpretation of the experiment consisted in comparing the calculated CPSDs values with the measured ones, showing that, in absolute terms, the results provided by the model are in good agreement with the experiments, for both amplitude and phase. When comparing the CPSDs ratios, as done in other works within the project, the model well agrees within the experimental uncertainties, proving the accuracy of the presented methodology. Additional interpretations and parametric analyses are foreseen as the next steps of the development and the application of the code.

ACKNOWLEDGMENTS

The CORTEX project received funding from the Euratom Research and Training Programme 2014-2018 under grant agreement No 754316. The CEA team would like to thank the EPFL team for providing their experimental results and for the fruitful discussions during all project activities.

REFERENCES

[1] V. Lamirand, A. Rais, S. Hübner, C. Lange, J. Pohlus, U. Paquee, C. Pohl, O. Pakari, P. Frajtag, D. Godat, M. Hursin, A. Laureau, G. Perret, C. Fiorina and A. Pautz, "Neutron noise experiments in the AKR-2 and CROCUS reactors for the European project CORTEX," *ANIMMA 2019, EPJ Web of Conferences 225, 04023 (2020),* 2019, https://doi.org/10.1051/epjconf/202022504023.

[2] O. Pakari, V. Lamirand, G. Perret, L. Braun, P. Frajtag and A. Pautz, " Current Mode Neutron Noise Measurements in the Zero Power Reactor CROCUS," *EPJ Web of Conferences,* vol. 170, p. 2018.

[3] A. G. Mylonakis, C. Demazière, P. Vinai, V. Lamirand, A. Rais, O. Pakari, P. Frajtag, D. Godat, M. Hursin, G. Perret, A. Laureau, C. Fiorina and A. Pautz, "CORE SIM+ simulations of COLIBRI fuel rods oscillation experiments and comparison with measurements," in *PHYSOR 2020: Transition to a Scalable Nuclear Future*, Cambridge, United Kingdom, March 29th-April 2nd, 2020.

[4] V. Lamirand, P. Frajtag, D. Godat, M. Hursin, G. Perret, O. Pakari, A. Rais, C. Fiorina and A. Pautz, "The COLIBRI programme in CROCUS : characterisation of the fuel rods oscillator," *ANIMMA 20199, EPJ Web of Conferences 225, 04020 (2020),* 2019, https://doi.org/10.1051/epjconf/202022504020.

[5] S. Santandrea, D. Sciannandrone, R. Sanchez, L. Mao and L. Graziano, "A Neutron Transport Characteristics Method for 3D Axially Extruded Geometries Coupled with a Fine Group Self-Shielding Environment," *Nuc. Sci. Eng.,* vol. 186, no. 3, pp. 239-276, 2017.

[6] V. Lamirand, M. Hursin, A. Rais, S. Hubner, C. Lange, J. Pohlus, U. Paquee, C. Pohl, O. Pkari and A. Laureau, "Experimental Report of the 1st campaign at AKR-2 and CROCUS," CORTEX - D2.1, 03 Dec. 2018.

[7] V. Lamirand, *Private communications,* 31 Jan. 2020.

[8] V. Lamirand, A. Rais, O. Pakari, M. Hursin, A. Laureau, J. Pohlus, U. Paquee, C. Pohl, S. Hubner, C. Lange, P. Frajtag, D. Godat, G. Perret, C. Fiorina and A. Pautz, "Analysis of the first COLIBRI neutron noise campaign in the CROCUS reactor for the European project CORTEX," in *PHYSOR2020: Transition to a Scalable Nuclear Future*, Cambridge, United Kingdom, March 29th-April 2nd, 2020.

[9] S. Santandrea, L. Graziano and D. Sciannandrone, "Accelerated polynomial axial expansion for full 3D neutron transport MOC in APOLLO3® code system as applied to the ASTRID fast breeder reactor," *Ann. Nuc. Energy,* vol. 113, pp. 194-236, 2018, https://doi.org/10.1016/j.anucene.2017.11.010.

[10] S. Santandrea, L. Graziano, I. Zmijarevic and B. Vezzoni, "A Leakage synthetic algorithm and a Krylov approach for thermal iterations in APOLLO3 code in support to industrial applications," *submitted to ANS M&C 2021 Conference.*

[11] A. Brighenti, S. Santandrea, I. Zmijarevic and Z. Stankovski, "Interpretation of COLIBRI measurements in the CROCUS research reactor using a point-kinetics reactor model," *submitted to the PHYTRA5 conference,* 2020.

[12] A. Gammicchia, S. Santandrea, I. Zmijarevic, R. Sanchez, Z. Stankovski, S. Dulla and P. Mosca, "A MOC-based neutron kinetics model for noise analysis," *Ann. Nucl. Energy,* vol. 137, 2019.

[13] A. F. Henry, Nuclear-Reactor Analysis, Cambridge (MA): The MIT Press, 1986.

[14] S. Dulla, E. H. Mund and P. Ravetto, "The quasi-static method revisited," *Prog. Nucl. Energ.,* vol. 50, no. 8, pp. 908-920, 2008.

[15] F. B. Hildebrand, Introduction to numerical analysis (second edition), New York: Dover Publications Inc., 1987.

[16] D. L. Hetrick, Dynamics of Nuclear Reactors, The University of Chicago Press, 1971.

[17] A. Santamarina, D. Bernard, P. Blaise, M. Coste, A. Courcelle, T. Huynh, C. Jouanne, P. Leconte, O. Litaize, S. Mengelle, G. Noguère, J. M. Ruggiéri, O. Sérot, J. Tommasi, C. Vaglio and J. F. Vidal, "The JEFF-3.1.1 nuclear library," Technical Report JEFF Report 6807, 2009.

Appendix A
Construction of matrix operators

The IPK model presented is written using matrix operators in the form:

$$(\mathcal{T} + \mathcal{S}_t + \mathcal{R} - \mathcal{H})P = \frac{1}{k_{dyn}}(\mathcal{F}_p + \mathcal{F}_d)P \tag{16}$$

It is necessary that the formulation keeps an explicit energy dependence of P in all the equations. In this section, the operators' construction will be presented considering M times-step and N_g energy groups. In each indication of row or column of the matrix, the value $i = M \cdot (g-1)$ and $j = M \cdot (g'-1)$, where g and g' are two generic energy groups.

A.1 The time discretization operator $\mathcal{T}$

With the normalization condition of Eq. (7) , the operator $\mathcal{T} = \frac{1}{v_g}\langle \psi_g^\dagger, S_g \rangle \partial_t$ reduces to $\mathcal{T} = \partial_t$, in which the time derivative is discretized using 4-th order finite difference on the generic time instant m:

$$\left(\frac{\partial f}{\partial t}\right)_m = \frac{f_{m-2} - 8f_{m-1} + 8f_{m+1} - f_{m+2}}{\delta t} \tag{17}$$

Therefore the element of matrix T are defined as:

$$\begin{gathered} \mathcal{T}(i+m, i+m) = 0 \\ \mathcal{T}(i+m, i+m-2) = 1/12\delta t \\ \mathcal{T}(i+m, i+m-1) = -8/12\delta t \\ \mathcal{T}(i+m, i+m+1) = 8/12\delta t \\ \mathcal{T}(i+m, i+m+2) = -1/12\delta t \end{gathered} \tag{18}$$

Taking advantage to the periodicity of the phenomenon, it is possible to couple the first two rows with the last two rows, and vice versa, by knowing that $t_1 = t_M + 1$ and $t_2 = t_M + 2$.

A.2 The shape derivative operator $\mathcal{S}_t$

In the operator $\mathcal{S}_t = \frac{1}{v}\langle \psi^\dagger, \partial_t S \rangle$ the derivative is evaluate using a first order finite difference. The operator is diagonal and computed using the interpolated shape at $\vec{x}_g = (\vec{r}, E_g, \Omega)$ and, considering the discrete time t_m, it is expressed as:

$$\begin{gathered} \mathcal{S}_t(i+m, i+m) = \\ = \frac{1}{v_g}\int_V d\vec{r} \int_\Omega d\Omega' \, \psi^\dagger(\vec{x}_g, t_m) \sum_{i=1}^{N/2} a_i(\vec{x}_g) \cos\left(\frac{2\pi}{T} t_m\right) + b_i(\vec{x}_g) \sin\left(\frac{2\pi}{T} t_m\right) \end{gathered} \tag{19}$$

A.3 The removal operator $\mathcal{R}$

The operator $\mathcal{R} = \langle \psi^\dagger, \tilde{\Sigma}_t S \rangle$ accounts for neutron losses due to removal, axial and radial leakages. It is diagonal and using the scalar shape (i.e. integrated in angle), for the discrete time t_m, it is written as:

$$\mathcal{R}(i+m, i+m) = \int_V d\vec{r} \int_\Omega d\Omega' \, \psi^\dagger(\vec{x}_g, t_m) \tilde{\Sigma}_t(\vec{r}, E_g, t_m) S(\vec{x}_g, t_m) \tag{20}$$

A.4 The scattering operator $\mathcal{H}$

The scattering operator is expressed by:

$$\mathcal{H} = \langle \psi^{\dagger}, HS \rangle = \langle \psi^{\dagger}, \int_E dE' \int_\Omega d\Omega' \, \Sigma_s(\vec{r}, \Omega' \to \Omega, E' \to E, t) S(\vec{r}, E', \Omega', t) \rangle \tag{21}$$

Writing the scattering cross section as an expansion of scattering moments on Legendre polynomials:

$$\begin{aligned} \Sigma_s(\vec{r}, \Omega' \to \Omega, E' \to E, t) &= \sigma_s(\vec{r}, E, t) f_s(\vec{r}, E' \to E, \mu_0) = \\ &= \sum_{l=0}^{\infty} \frac{2l+1}{4\pi} \sigma_l(\vec{r}, E' \to E, t) P_l(\mu_0) \end{aligned} \tag{22}$$

Where $\mu_0 = \Omega' \cdot \Omega$ and the expansion coefficients $\sigma_l(\vec{r}, E' \to E, t)$ are given by:

$$\sigma_l(\vec{r}, E' \to E, t) = 2\pi \int_{-1}^{1} \sigma_s(\vec{r}, E, t) f_s(\vec{r}, E' \to E, \mu_0) P_l(\mu_0) d\mu_0 \tag{23}$$

Since in (23) scattering moments and functions are taken from library, (21) becomes:

$$\begin{aligned} \mathcal{H} = \langle \psi^{\dagger}, HS \rangle = \\ = \langle \psi^{\dagger}, \sum_{l=0}^{\infty} \frac{2l+1}{4\pi} P_l(\mu) \int_E \sigma_l(\vec{r}, E' \to E, t) \int_{-1}^{1} S(\vec{r}, E', \mu', t) P_l(\mu') \, d\mu' dE' \rangle \end{aligned} \tag{24}$$

Using a multi-group approach, defining the ingoing and outgoing energies defined as g' and g, respectively. Therefore at a given discrete time t_m, the scattering source in group g from group g' is defined by:

$$\begin{aligned} h_{g,g',m} = \int_V \psi^{\dagger}(\vec{x}_g, t_m) \cdot \\ \sum_{l=0}^{\infty} \frac{2l+1}{4\pi} P_l(\mu) \int_E \sigma_l(\vec{r}, E_{g'} \to E_g, t_m) \int_{-1}^{1} S(\vec{r}, E_{g'}, \mu', t_m) P_l(\mu') \, d\mu' dE' d\vec{r} = \end{aligned} \tag{25}$$

Therefore the final form of the scattering operator is:

$$\mathcal{H}(i+m, j+m) = h_{g,g',m} \tag{26}$$

A.5 The prompt fission operator $\mathcal{F}_p$

The prompt fission operator $\mathcal{F}_p = \langle \psi^{\dagger}, F_p S \rangle$ Considering $j = 1, \dots, N_{iso}$ fissile isotopes and the factorization of the delayed neutron fractions $\beta^j(E) = \bar{\omega}_d^j P_{ed}^j(E)$ [17], the neutrons produced by fission in group g' and emitted in group g can be computed as:

$$\mathcal{F}_p = \langle \psi^{\dagger}(\vec{x}, t), \sum_{j=1}^{N_{iso}} \chi_j^p(\vec{r}, E, t) \int_E dE' \left(1 - \bar{\omega}_d^j P_{ed}^j(E')\right) \nu \Sigma_{f,j}(\vec{r}, E', t) S(\vec{r}, E', t) \rangle \tag{27}$$

In the multi-group approach adopted here, the emission f_{g,g',t_m} of prompt neutrons in group g from a fission occurred in group g' at a given time t_m is obtained from:

$$f_{g,g',m} = \int_V \psi^\dagger(\vec{x}, t_m) \cdot \sum_{j=1}^{N_{iso}} \chi_j^p(\vec{r}, E_g, t_m) \int_E dE' \left(1 - \bar{\omega}_d^j P_{ed}^j(E_{g'})\right) \nu\Sigma_{f,j}(\vec{r}, E_{g'}, t_m)\, S(\vec{r}, E_{g'}, t_m)\, d\vec{r} \tag{28}$$

Where χ_j^p is the prompt emission spectra and $\nu\Sigma_{f,j}$ is the number of neutron produced by the fissions of the j-th isotope. Finally, the operator is built as:

$$\mathcal{F}_p(i+m, j+m) = f_{g,g',m} \tag{29}$$

A.6 The delayed fission operator $\mathcal{F}_d$

The operator $\mathcal{F}_d$ is built starting from the treatment in [12], where derivation of the quadrature formula for the delayed fission source is presented. For the here discretized problem, at a given discrete time t, the neutrons produced by fissions in group g' and emitted in group g:

$$d_{g,g',m} = \int_V \psi^\dagger(\vec{x}_g, t_m) \cdot \sum_{i=1}^{N_d} \lambda_i \chi_i^d(\vec{x}, E_g, t_m) \sum_{m'=1}^{M} \omega_{i,m'}(t_m) \beta_i(E_{g'}) \sum_{j=1}^{N_{iso}} \nu\Sigma_{f,j}(\vec{r}, E_{g'}, t_m)\, S(\vec{r}, E_{g'}, t_m)\, d\vec{r} \tag{30}$$

Where $\omega_{i,m'}$ are the weights of the quadrature formula, N_d is the number of delayed family precursors, λ_i is the decay constant and χ_i^d is the delayed emission spectra for the i-th family, respectively. Finally, the operator is built as:

$$\mathcal{F}_g(i+m, j+m) = d_{g,g',m} \tag{31}$$